

## Model-based localization of deep-diving cetaceans using towed line array acoustic data

Yvonne M. Barkley, Eva-Marie Nosal and Erin M. Oleson

Citation: *The Journal of the Acoustical Society of America* **150**, 1120 (2021); doi: 10.1121/10.0005847

View online: <https://doi.org/10.1121/10.0005847>

View Table of Contents: <https://asa.scitation.org/toc/jas/150/2>

Published by the [Acoustical Society of America](#)

---

### ARTICLES YOU MAY BE INTERESTED IN

[Separating overlapping echolocation: An updated method for estimating the number of echolocating animals in high background noise levels](#)

*The Journal of the Acoustical Society of America* **150**, 709 (2021); <https://doi.org/10.1121/10.0005756>

[Probabilistic focalization for shallow water localization](#)

*The Journal of the Acoustical Society of America* **150**, 1057 (2021); <https://doi.org/10.1121/10.0005814>

[A three-dimensional finite difference model for ocean acoustic propagation and benchmarking for topographic effects](#)

*The Journal of the Acoustical Society of America* **150**, 1140 (2021); <https://doi.org/10.1121/10.0005853>

[Bounding the number of calling animals with passive acoustics and reliable locations](#)

*The Journal of the Acoustical Society of America* **150**, 1496 (2021); <https://doi.org/10.1121/10.0004994>

[Near real-time detection of low-frequency baleen whale calls from an autonomous surface vehicle: Implementation, evaluation, and remaining challenges](#)

*The Journal of the Acoustical Society of America* **149**, 2950 (2021); <https://doi.org/10.1121/10.0004817>

[Generalized Radon transform approach to target motion parameter estimation using a stationary underwater vector hydrophone](#)

*The Journal of the Acoustical Society of America* **150**, 952 (2021); <https://doi.org/10.1121/10.0005813>

---

**JASA**  
THE JOURNAL OF THE  
ACOUSTICAL SOCIETY OF AMERICA

**Special Issue: Fish Bioacoustics:  
Hearing and Sound Communication**

CALL FOR PAPERS

## Model-based localization of deep-diving cetaceans using towed line array acoustic data

Yvonne M. Barkley,<sup>1,a)</sup> Eva-Marie Nosal,<sup>2</sup> and Erin M. Oleson<sup>3</sup>

<sup>1</sup>Hawai'i Institute of Marine Biology, School of Ocean and Earth Science and Technology, University of Hawai'i at Mānoa, Kāne'ohe, Hawaii 96822, USA

<sup>2</sup>Ocean Resources and Engineering, School of Ocean and Earth Science and Technology, University of Hawai'i at Mānoa, Honolulu, Hawaii 96822, USA

<sup>3</sup>Protected Species Division, Pacific Islands Fisheries Science Center, National Marine Fisheries Service, National Oceanic and Atmospheric Administration, Honolulu, Hawaii 96818, USA

### ABSTRACT:

Passive acoustic monitoring using a towed line array of hydrophones is a standard method for localizing cetaceans during line-transect cetacean abundance surveys. Perpendicular distances estimated between localized whales and the trackline are essential for abundance estimation using acoustic data. Uncertainties in the acoustic data from hydrophone movement, sound propagation effects, errors in the time of arrival differences, and whale depth are not accounted for by most two-dimensional localization methods. Consequently, location and distance estimates for deep-diving cetaceans may be biased, creating uncertainty in abundance estimates. Here, a model-based localization approach is applied to towed line array acoustic data that incorporates sound propagation effects, accounts for sources of error, and localizes in three dimensions. The whale's true distance, ship trajectory, and whale movement greatly affected localization results in simulations. The localization method was applied to real acoustic data from two separate sperm whales, resulting in three-dimensional distance and depth estimates with position bounds for each whale. By incorporating sources of error, this three-dimensional model-based approach provides a method to address and integrate the inherent uncertainties in towed array acoustic data for more robust localization.

© 2021 Acoustical Society of America. <https://doi.org/10.1121/10.0005847>

(Received 29 January 2021; revised 3 June 2021; accepted 19 July 2021; published online 12 August 2021)

[Editor: Klaus Lucke]

Pages: 1120–1132

### I. INTRODUCTION

Passive acoustic monitoring (PAM) is commonly used to study the ecology and behavior of cetacean species using their vocalizations. The role of cetaceans as top predators and ecosystem sentinels (Moore, 2008; Bossart, 2011; Hazen *et al.*, 2019) makes it critical to obtain baseline data for these species to be able to detect changes in their distributions and abundance (Davis *et al.*, 2017; Gibb *et al.*, 2019). Over the past decade, advances in methods to detect and classify cetacean sounds (Bittle and Duncan, 2013) have allowed for passive acoustic data to be incorporated into an increasing number of studies that model species distributions and estimate abundance of cetacean populations (Marques *et al.*, 2009; Marques *et al.*, 2013; Fleming *et al.*, 2018; Harris *et al.*, 2018). Passive acoustic data have also provided important information about cryptic and deep-diving cetacean species in the absence of other data types (e.g., visual observations, telemetry data) to inform conservation and management decisions (Carlén *et al.*, 2018; Hodge *et al.*, 2018; Hildebrand *et al.*, 2019).

Localization methods for acoustic data vary depending on the application and design of the PAM system. Several

types of towed hydrophone systems exist (Marques *et al.*, 2013; Zimmer, 2013), but short-aperture towed line arrays are widely used as a standard method to track and localize vocalizing cetaceans during shipboard visual and acoustic line-transect surveys (Van Parijs *et al.*, 2009; Rankin *et al.*, 2013; Yano *et al.*, 2018). The surveys are designed to estimate cetacean abundance based on distance sampling methods. Distance sampling allows for an estimation of the number of missed detections by calculating the detection probability as a function of the perpendicular distances measured between objects (e.g., cetaceans) and the trackline (Buckland *et al.*, 2001). The detection function is typically comprised of distance measurements from visual observations and is assumed to be accurate for reliable abundance estimates.

Passive acoustic data collected with short-aperture towed line arrays can also contribute distance estimates for cetaceans using target motion analysis (TMA). The time difference of arrival (TDOA) of a vocalization is calculated between a pair of hydrophones restricting the position of the vocalizing animal to a hyperbolic surface. However, TMA uses two-dimensional (2D) bearings to the vocalizing animal derived from the intersection of the hyperbolic surfaces with a plane at the depth of the towed line array. Over time, consecutive bearings will intersect as the animal passes 90°

<sup>a)</sup>Electronic mail: ybarkley@hawaii.edu, ORCID: 0000-0003-4251-474X.

of the ship, and a perpendicular distance can be measured from the array to the intersection point. (Lewis *et al.*, 2007; Rankin *et al.*, 2008). In theory, the estimated distances derived from 2D TMA provide an opportunity for acoustic-based abundance estimation. However, the method operates under assumptions that are frequently violated in practice, including that the hydrophone positions are perfectly known, the sound speed is constant, and the vocalizing whales are mostly stationary at the same depth as the array. The perpendicular distances estimated with 2D TMA are often point estimates and do not account for the three-dimensional (3D) environment of the whales and the effects of depth when calculating distances. Additionally, errors associated with sources of uncertainty, such as inaccuracies in TDOA measurements, hydrophone movement, variation in sound speed profiles, or whale movement, are usually not accounted for in the simplistic framework of 2D TMA.

Deep-diving cetaceans, such as sperm whales and beaked whales, do not conform to the assumptions of 2D TMA since they primarily vocalize (echolocate) at depths hundreds of meters below the towed line array (Teloni *et al.*, 2008; Schorr *et al.*, 2014). This can lead to inaccuracies in perpendicular distance estimates, particularly overestimating distances for whales located deeper in the water column and closer to the ship. While Barlow and Taylor (2005) found that the depths of sperm whales did not significantly affect abundance estimates when using a line array towed at 100 m depth, only point estimates for distances were provided, and it is unclear whether the same conclusions apply in all conditions (e.g., line arrays towed at shallower depths or in different ocean environments).

Other localization studies of deep divers detected using towed line array data incorporated surface reflections to overcome the uncertainty introduced by depth. Thode (2004) used surface reflections to simultaneously track dive profiles of sperm whales within close range. The method required slowly towing a wide-aperture tandem array consisting of two staggered line arrays (170-m maximum hydrophone spacing). The slow speeds (~3.7 km/h) allowed the array to sink deep enough to accurately identify the reflections of the long-duration, multipulsed echolocation clicks ( $\geq 10$  ms; Møhl *et al.*, 2003). DeAngelis *et al.* (2017) estimated the depths of beaked whales using surface reflections from PAM data collected with a single short-aperture line array (~30 m maximum hydrophone spacing) that was more maneuverable for towing at typical line-transect survey speeds (~18.5 km/h). Faster towing speeds resulted in an average array depth of 13 m, which was appropriate for identifying surface reflections of short-duration echolocation clicks ( $\leq 0.8$  ms; Baumann-Pickering *et al.*, 2013). Reflections are undeniably useful for estimating depths of diving whales (Zimmer *et al.*, 2008), but their presence relies heavily on the configuration of the PAM system and the vocal characteristics of the species, making it difficult to accurately distinguish them in some data sets.

Model-based localization provides an approach to incorporate sound propagation effects, account for the depth

of diving cetaceans, and incorporate sources of uncertainty to provide error estimates. This technique was originally applied to track and localize whales using widely spaced bottom-mounted hydrophone arrays (Tiemann *et al.*, 2004; Nosal and Frazer, 2006; Warner *et al.*, 2017). Thode (2005) implemented a model-based approach using a towed tandem array to account for sound propagation effects while tracking and localizing sperm whales at close range. To our knowledge, however, model-based methods have not been broadly applied to localize acoustic data acquired from short-aperture towed line arrays. Instead, 2D TMA continues to be the common localization method for this type of acoustic data, which is suitable for certain species that are relatively stationary and detected at the same depth as the line array. However, assumptions are violated when localizing deep-diving species, and continuing to use 2D TMA perpetuates the use of potentially biased distance and location estimates without providing a method to quantify error.

Here, we develop a semi-automated localization method that adapts a model-based approach to localize sperm whales using single short-aperture towed line array data collected during line-transect surveys. Our method localizes in three dimensions, incorporates sources of uncertainties, accounts for sound propagation effects, and provides position bounds for stationary and moving animals. We demonstrate the method in a simulation study to examine several parameters that affect localization results. We then implement the method to localize two real acoustic encounters of sperm whales and discuss the benefits and limitations of adapting the model-based approach to towed line array acoustic data.

## II. THEORY

### A. Ambiguity volumes

Our method modifies the model-based localization methods that have been successfully used for fixed hydrophones (Tiemann *et al.*, 2004; Nosal and Frazer, 2007; Gebbie *et al.*, 2015) and applies them to acoustic data collected using mobile line arrays (Fig. 1) to estimate the location and distance of whales from the trackline. Probabilistic indicators of source location, known as ambiguity volumes, are constructed by comparing measured and modeled TDOAs to estimate the location of the source (i.e., the estimated source location is the location at which modeled TDOAs best match measured TDOAs). Modeled TDOAs are generated using a sound propagation model to account for depth-dependent sound speed (Nosal, 2013).

For a hydrophone pair, modeled TDOAs are compared to the measured TDOAs to compute the ambiguity volumes,  $V$ , where  $V$  is given by

$$V(\mathbf{x}) = \prod_j V_j(\mathbf{x}) = \prod_j e^{-(1/2\sigma_j^2)(\overline{\Delta t_j}(\mathbf{x}) - \Delta t_j)^2}, \quad (1)$$

where  $\mathbf{x} = (x, y, z)$  is the 3D Cartesian coordinate of the candidate source locations,  $\overline{\Delta t_j}(\mathbf{x})$  is the modeled TDOA at

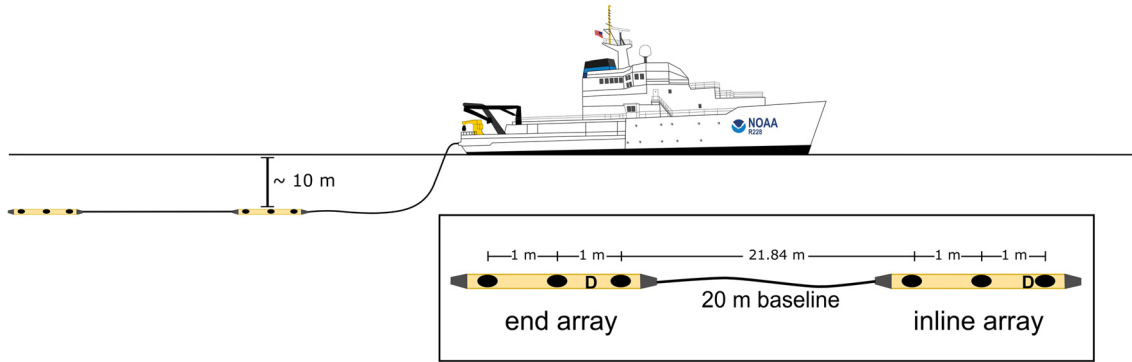


FIG. 1. (Color online) Diagram of the line array towed 300 m behind the NOAA research vessel, NOAA ship *Reuben Lasker*, at approximately 10 m deep during a cetacean abundance line-transect survey in 2017. The line array consisted of two depth sensors (denoted with “D”) and two array nodes spaced 20 m apart, each housing three hydrophones (black dots) spaced approximately 1 m apart.

candidate source location  $x$ , and  $\Delta t_j$  is the measured TDOA. The product in Eq. (1) is over detection number, where the index  $j$  corresponds to detections from different positions along the ship trackline that are associated with a single whale (or closely spaced group of whales) (Fig. 2) and  $V_j(x)$  is the individual ambiguity volume corresponding to click  $j$ . This is a form of TMA whereby a wide baseline system is artificially created by moving a short baseline array through the environment and assumes that  $V_j(x)$  are independent measurements. As  $V_j(x)$  are multiplied, areas of high value that overlap are reinforced, resulting in a higher value of  $V(x)$ , while areas that do not overlap result in lower  $V(x)$  values. The whale position is estimated at the position  $x$ , which maximizes values of  $V(x)$  across the entire space.

The total uncertainty is incorporated through sigma,  $\sigma_t$ , which accounts for uncertainty in TDOA, sound speed profile, and hydrophone position,

$$\sigma_t = \sqrt{\sigma_a^2 + \sigma_b^2 + \sigma_c^2}, \quad (2)$$

where  $\sigma_a$  is the standard deviation in the measured TDOAs,  $\sigma_b$  is the standard deviation due to uncertainty in hydrophone position (introduced by hydrophone movement), and  $\sigma_c$  is standard deviation due to sound speed uncertainty. For the simulations and data presented below, we used  $\sigma_a = 0.001$  s,  $\sigma_b = 0.002$  s, and  $\sigma_c = 0.001$  s.  $\sigma_a$  was based on the peak width (at the noise floor) of the envelopes (computed via Hilbert transform) of the cross correlation functions computed from a sample of noisy echolocation clicks.

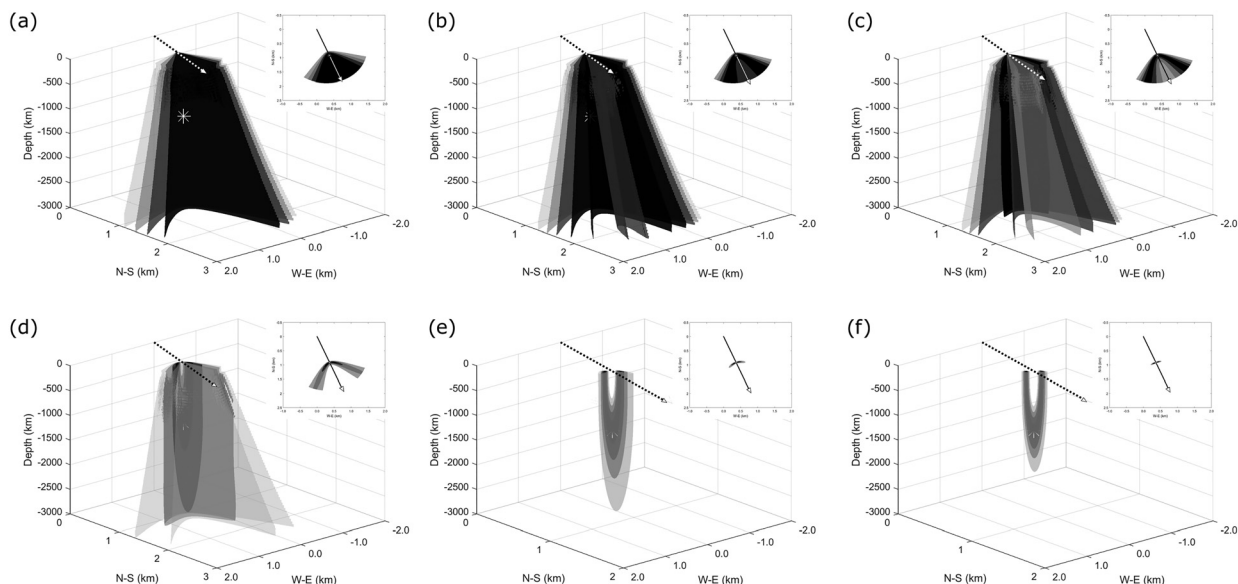


FIG. 2. Cumulative ambiguity volumes [(a)–(f)] for detections of simulated echolocation clicks from a stationary whale located 1.2 km directly below the transect line (denoted by a white asterisk). The product of all volumes results in a volume representing all possible location estimates for the whale (f). The color scale represents the ambiguity volume values ranging from 0 (white) as low probability to 1 (black) as high probability. The dotted lines (white or black) indicate the trackline traveling in the direction of the arrow.

$\sigma_b$  was estimated based on a maximum (empirically determined) hydrophone movement of 3 m and an average sound speed of 1500 m/s.  $\sigma_c$  was estimated by executing the BELLHOP model (Porter and Liu, 1994; Porter, 2011) multiple times over a collection of typical sound speed profiles and then taking the maximum difference between the resulting TDOAs.

Position bounds are estimated by profiling the ambiguity volumes. The profiled ambiguity volume along the  $x$ -dimension is defined as

$$VP(x) = \max_{y,z} V(x), \tag{3}$$

where position bounds in  $x$  are defined by the  $x$ -positions that encompass the estimated whale position at which  $VP(x)$  falls below a threshold. Position bounds in  $y$  and  $z$  are estimated analogously. To estimate bounds on the whale's distance from the trackline, profiling of the ambiguity volume is applied relative to the perpendicular line that extends from the trackline and passes through the estimated whale location. Position bounds were calculated for distance and depth from the profiled ambiguity volumes using 95% confidence intervals.

### B. Simulation experiment

We demonstrate the application of the model-based localization approach in a simulation to estimate the location and distance of a foraging sperm whale detected at depth using a short-aperture towed line array. Simulations and data analyses were performed with customized routines using MATLAB (2018). Sperm whales produce four types of clicks depending on their behavior and group composition. The click types can be characterized by their interclick interval (ICI), which is the rate at which the clicks are

produced (Whitehead and Weilgart, 1990; Jaquet *et al.*, 2001; Marcoux *et al.*, 2006; Watwood *et al.*, 2006). Codas are repeated stereotyped sequences of clicks lasting approximately 3 s with ICIs that are highly variable and group-specific (Rendell and Whitehead, 2004; Gero *et al.*, 2016; Oliveira *et al.*, 2016). Regular clicks (0.5–1.2 s ICI) and creaks (0.01–0.1 s ICI) are associated with echolocation and foraging (Jaquet *et al.*, 2001; Miller *et al.*, 2004; Hildebrand, 2005; Watwood *et al.*, 2006), while slow clicks are produced primarily by male sperm whales (>2 s ICI; Madsen *et al.*, 2002; Oliveira *et al.*, 2013). For the purposes of this study, a 15-min encounter was simulated for a whale producing regular clicks by generating 500 click times drawn from a standard uniform distribution on the interval (0 s, 900 s). The parameters assumed a longer ICI for regular clicks (1.8 s) to account for clicks that could be missed due to whale orientation, sound propagation, or acoustic masking. The simulated whale position was fixed at a known distance and depth relative to the line array, assuming whale movement to be negligible during the 15 min. The simulated line array was placed at an average depth of 10 m while towed 300 m behind a ship traveling at 18.5 km/h. Hydrophone spacings within the array were equivalent to the towed line arrays used for line-transect cetacean surveys illustrated in Fig. 1. All simulations used the Gaussian beam acoustic propagation model BELLHOP (Porter and Liu, 1994; Porter, 2011) passed through a representative sound speed profile of Hawaiian waters to create a lookup table of predicted arrival times for computing the acoustic ray paths (Fig. 3). The representative sound speed profile combined averaged *in situ* data for depths up to 1 km collected during research surveys on September 2, 2017 and November 18, 2017, with historic data from the 2013 World Ocean Atlas (Boyer *et al.*, 2013) for depths below 1 km [Fig. 3(a)].

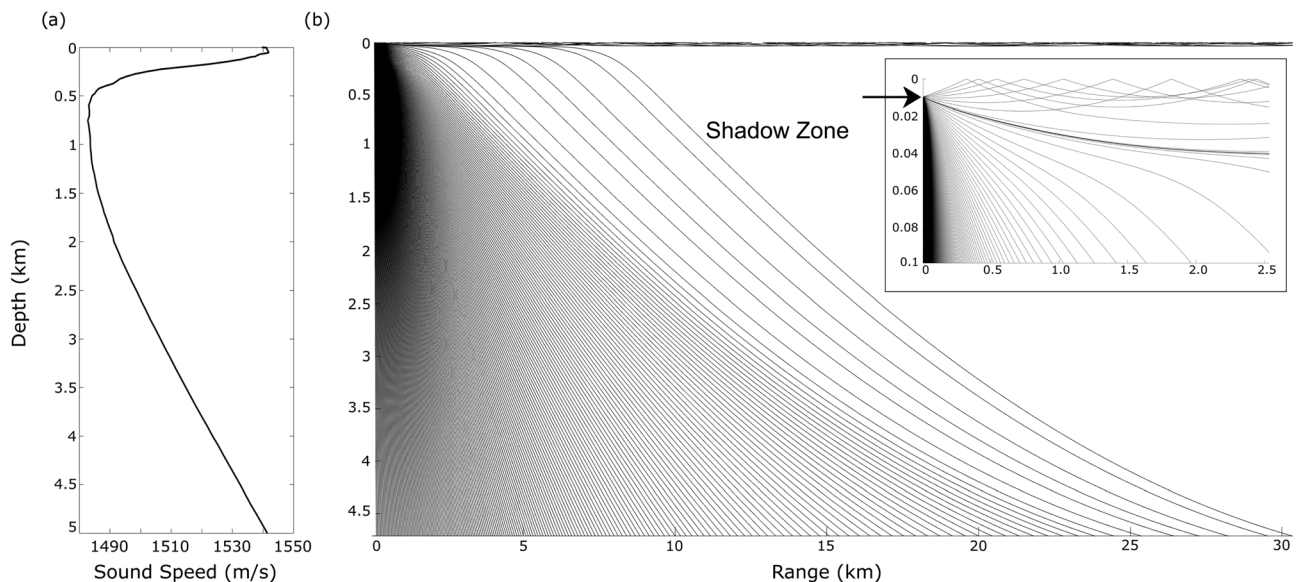


FIG. 3. Sound speed profile (a) and ray traces (b) for the Hawaiian waters study area incorporated into the simulation study. The white space represents the shadow zone. The inset shows the upper 100 m with a receiver at 10 m denoted with a black arrow. Note that in reality, the receiver (array) is at 10 m, while the animal is at depth, but we apply the principle of reciprocity (i.e., the ray path is the same from source to receiver and vice versa) to simplify our modeling and illustration.

The click generation times, hydrophone positions, whale positions, and sound speed profile were used to simulate the TDOAs. Gaussian distributed white noise ( $\mu = 0$ ,  $\sigma = 0.012$ ) was added to the simulated TDOAs to mimic the noise in real towed array data.

To compute  $V(\mathbf{x})$ , we reduced the set of simulated TDOAs by smoothing over 1-min increments, resulting in one  $V_j(\mathbf{x})$  approximately every 300 m. This strategy assured independence between measurements while reducing noise and maintaining the overall pattern in the TDOAs. The spatial grid had horizontal and vertical spacing of 50 m, with depth dimension constrained to 2 km to account for the deepest measured dive depths of sperm whales (Teloni *et al.*, 2008; Oliveira *et al.*, 2013; Irvine *et al.*, 2017).

An ambiguity volume represents all possible locations of the detected whale within a probability range, but the shape of this volume depends on the distance and depth of the whale, the ship trajectory, sound propagation effects, and the overall uncertainty ( $\sigma_t$ ). To evaluate the effects of these variables on localization results, we included them in different combinations to simulate realistic scenarios based on line-transect survey design and sperm whale behavior (Table I). Ship trajectory is important since location estimates for whales detected along a straight ship trajectory are subject to left/right ambiguity, which can only be resolved by turning the ship. We included two types of ship trajectories, “straight” or “turn,” to examine the effects on the ambiguity surfaces. For scenarios with a turn, we tested three turn angles (20°, 60°, 80°) representing a low, medium, and high degree of change in the direction of the ship during a survey. Simulated turns consisted of a straight segment of trackline followed by a segment of trackline offset by the selected turn angle. We allowed for the line array to straighten out by calculating TDOAs 5 min after the turn was completed. In addition, simulations included the whale as stationary for the duration of the encounter or moving in one direction relative to the ship. In both cases, the whale’s initial position was placed at a perpendicular distance and depth representative of the detection range of sperm whales using a towed line array (Barlow and Taylor, 2005; Teloni *et al.*, 2008).

It is particularly challenging to localize a stationary whale when it is detected directly below a ship traveling straight along the trackline (Figs. 2 and 4). 2D TMA does not consider the depth of the whale and, therefore, automatically estimates it to be some distance from the trackline that is approximately equivalent to the whale’s depth. A simulation of a whale located 1.1 km below the ship resulted in a U-shaped ambiguity volume where the whale could theoretically be located at any point within the volume [Fig. 4(1a)].

The ambiguity volume was maximized [ $V(\mathbf{x}) = 0.98$ ] at a distance of 0.25 km from the trackline (left/right ambiguous), and distance was bounded by [0, 1.4] km [Fig. 4(1b)]. The maximum  $V(\mathbf{x})$  occurred at a depth of 1.1 km with depth bounded by [0, 1.5] km [Fig. 4(1c)]. Although the simulation provided an apparent “best” position (distance = 0.25 km and depth = 1.1 km), this is an artefact created by the limitations of the ship trajectory (straight trackline), the noise introduced to the system, and the grid spacing used in the search. In reality, for this scenario, there are infinitely many points along the U-shaped volume with ambiguity values near the maximum value. Consequently, the position cannot be further refined (beyond the U-shaped volume) given a straight trackline without the use of surface reflections or other information.

The ambiguity and overall bounds on distance and depth estimates can be reduced if a turn is implemented during the encounter once the TDOAs reach 0 s, indicating the whale has passed 90° of the line array [Figs. 4(2a)–4(2c)]. For example, a 60° turn in the ship’s trackline resulted in a more constrained ambiguity volume encompassing all possible whale locations with a best distance estimate below the trackline (0 km) at 1.1 km depth with distance bounded by [0, 1.2] km and depth bounded by [0.45, 1.7] km [Figs. 4(2b) and 4(2c)]. The resulting ambiguity volume provided a more precise location estimate for the whale by turning the ship, reducing the possible distances of the location estimate for a whale located directly below the trackline.

Turning the ship also improved the precision of localizations for stationary whales located farther from the trackline. For example, localizing a whale positioned 4 km away at 1.1 km depth under a straight trackline simulation created two cylindrical ambiguity volumes with an estimated distance of 4.0 [2.3, 8.0] km (left/right ambiguous) and depth of 1.5 [0, 2.0] km error [ $\max V(\mathbf{x}) = 0.99$ ; Figs. 5(1a)–5(1c)]. The 60° turn reduced the ambiguity volume entirely to one side and estimated that the whale was at a distance of 4 [3.3, 5.2] km and a depth of 1.3 [0, 2.0] km [ $\max V(\mathbf{x}) = 0.97$ ; Figs. 5(2a)–5(2c)]. Overall, turning the ship reduced the volume of the ambiguity volume for whales closer and farther away from the trackline in different ways. Changing the ship trajectory greatly decreased the 3D ambiguity in distance estimates for whales detected below the trackline and resolved it completely for whales detected farther away. However, the bounds on depth remained large, especially for the farther whale. If they are available, surface reflections can be incorporated using the same framework and would further constrain depth estimates.

Simulations thus far have treated the whale as a stationary sound source. As with any TMA method, an

TABLE I. List of parameters included in combinations for the simulation study. NA, not applicable.

Ship trajectory	Turn angles (deg)	Whale perpendicular distance (m)	Whale depth (m)	Whale behavior
Straight	NA	0–7000	400–2000	Stationary, moving
Turn	20, 60, 80	0–7000	400–2000	Stationary, moving

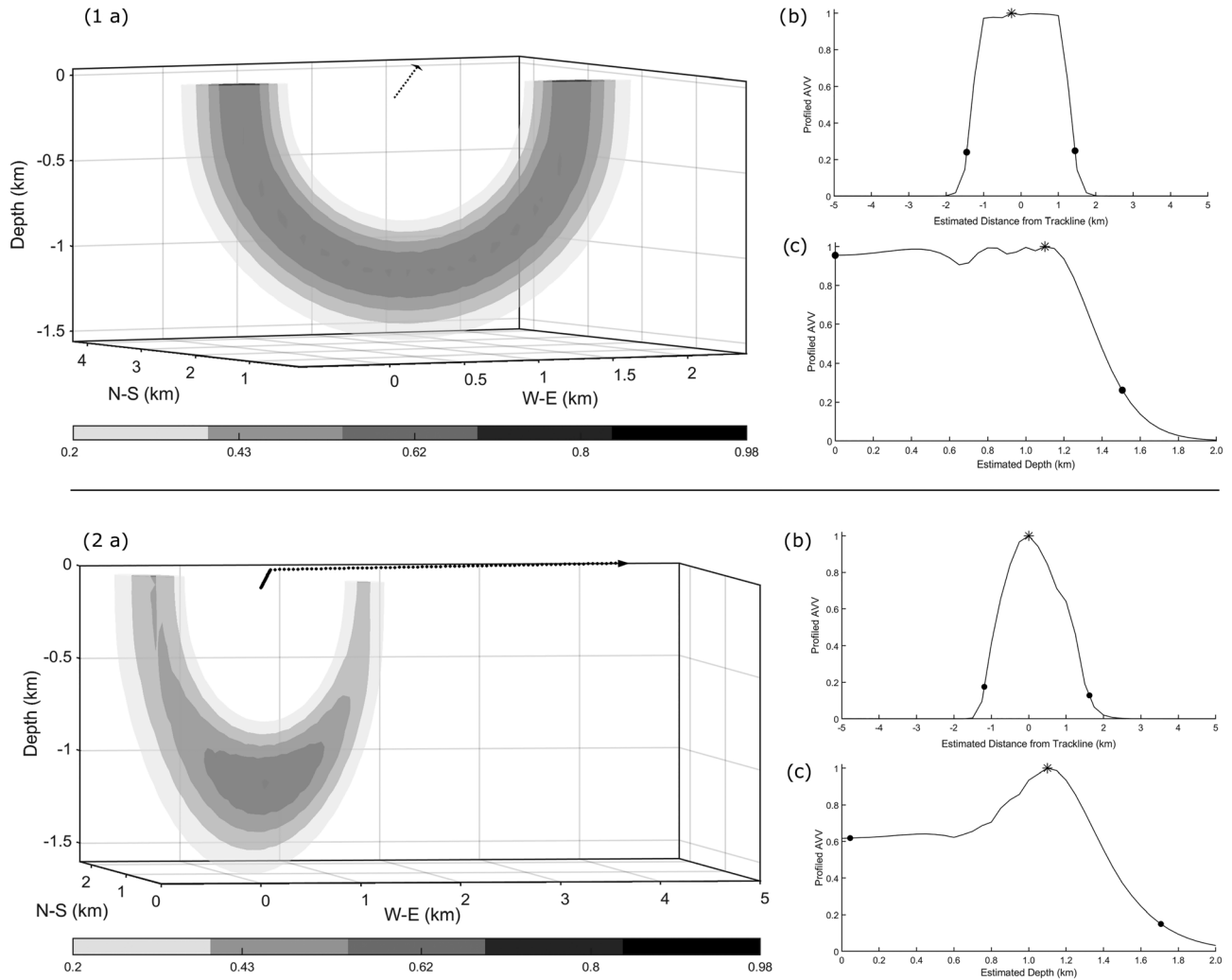


FIG. 4. Simulations of a whale detected 1.1 km below a ship traveling straight along the trackline produced a U-shaped ambiguity volume (1a), resulting in a left/right ambiguous distance estimate of 0.25 km with distance bounds of [0, 1.4] km (1b) and a depth estimate of 1.1 km with a depth bound of [0, 1.5] km (1c). Implementing a 60° turn reduced the ambiguity volume (2a), resulting in a distance estimate of 0 km (2b) and depth estimate of 1.1 km (2c) with position bounds of [0, 1.2] km and [0.45, 1.7] km, respectively. The gray scale represents the ambiguity volume values ranging from a low probability (light gray) to high probability (black, obscured “inside” the volume, hence not visible here). The position bounds are denoted with black dots on the profiled volumes [(b), (c)]. The black dotted lines indicate the ship’s trackline traveling in the direction of the arrow (a).

important limiting assumption of this approach is that the whales are stationary relative to the array during the encounter. In reality, a whale is likely moving as it vocalizes while traveling, foraging, or socializing, causing a violation of assumptions behind the calculation of  $V(\mathbf{x})$ .  $V_j(\mathbf{x})$  no longer overlap in space and therefore no longer reinforce each other at the whale position(s). We developed a strategy to incorporate the effects of whale movement by spatially dilating  $V_j(\mathbf{x})$  before combining them in  $V(\mathbf{x})$ . This is a conservative approach resulting in larger position bounds that are more appropriate when the assumptions are violated.

A local maximum dilation operator (Gonzalez *et al.*, 2009) was applied to each  $V_j(\mathbf{x})$  to encompass the maximum possible distance the whale may have traveled in any direction during the encounter. The dilation of an ambiguity volume  $V_j(x, y, z)$  was defined as

$$\begin{aligned}
 (V_j \oplus B)(x, y, z) &= \max\{V_j(x - x', y - y', z - z') \mid (x', y', z') \in D_B\},
 \end{aligned}
 \tag{4}$$

where  $D_B$  is the domain of the “filter” volume  $B$ .  $V_j \oplus B(\mathbf{x})$  is the maximum amplitude over all points in the neighborhood of  $\mathbf{x}$ ; regions with higher amplitudes in  $V_j(\mathbf{x})$  are enlarged in  $V_j \oplus B(\mathbf{x})$  proportionally to the size of  $B$ . The filter size and shape were an ellipsoid defined in proportion to averaged horizontal and vertical whale swim speeds of 0.5 and 1.13 m/s, respectively (Wahlberg, 2002), multiplied by the maximum time between each detection and the time of detection occurring 90° to the array (corresponding to TDOA = 0 s). Hence, it dilated  $V_j(\mathbf{x})$  according to the maximum possible swim distance for detection  $j$  within the encounter.

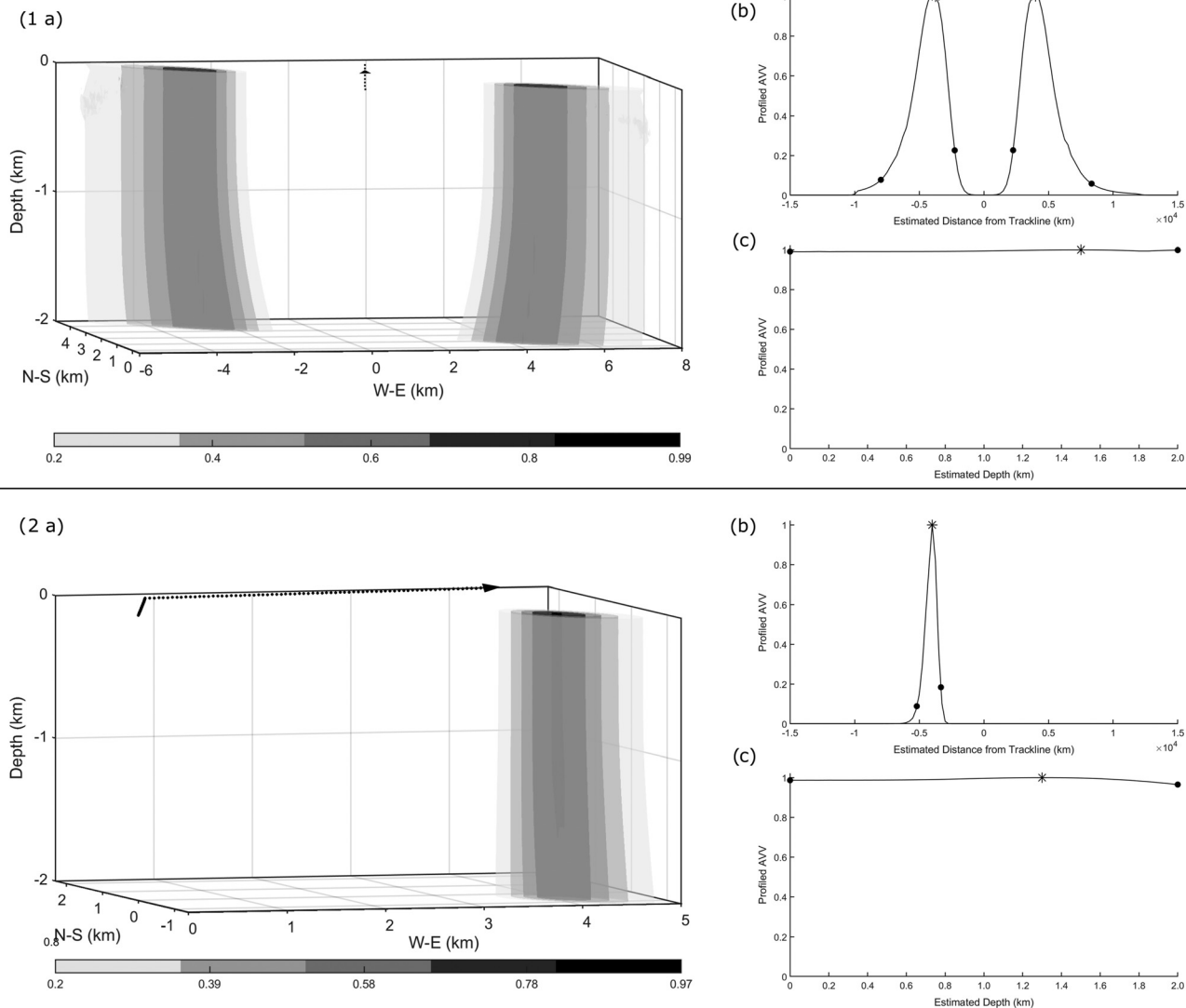


FIG. 5. Simulations of a stationary whale located 4 km from the straight trackline produced separate cylindrical ambiguity volumes (1a) resulting in a left-right ambiguous distance estimate of 4.0 km with a distance bound of [2.3, 8.0] km (1b) and a depth estimate of 1.5 km depth bound of [0, 2.0] km (1c). Implementing a 60° turn reduced the ambiguity volume (2a), resulting in a distance estimate of 4 km (2b) and depth estimate of 1.3 km (2c) with decreased position bounds of [3.3, 5.2] km and [0, 2.0] km, respectively.

We simulated two 15-min encounters of separate diving whales with the same initial distances and depths as the whales in the previous examples but changed the whales' positions at each time step to evaluate the performance of the localization algorithm for a moving whale. Thus, each click time was associated with a different 3D whale position. The whale positions changed based on an average swim speed of 1.2 m/s (Wahlberg, 2002; Aoki *et al.*, 2007) in a constant direction of travel with a slowly varying vertical component to simulate a dive pattern. The directions of travel included toward or away from the array as well as in the same or opposite direction relative to the array. As in the stationary whale simulations, the moving whale simulations used a straight trackline and a trackline with a 60° turn. Successful localization was defined when the ambiguity surface encompassed the whale's position at TDOA = 0 s, i.e., the time when the whale's location was perpendicular to the array, to ensure a more precise distance estimate.

Table II summarizes the results of these moving whale simulations that incorporated the dilation filter. For whales initially located at 0 km, the true distance of the whale at TDOA = 0 s (90° to the array) was captured within the distance bounds of the ambiguity volumes for each direction of movement in both the straight and turn scenarios. The distance estimates that maximized the ambiguity volume varied based on the direction of movement, ranging between 0 and 1 km. The largest distance bounds occurred for the straight and turn scenarios when the whale moved in the same direction as the array, [0, 2.2] and [0, 1.6] km, respectively. Overall, the distance bounds of all turn scenarios were less than the straight scenarios given the reduction of the ambiguity volume. Resulting distance estimates and bounds for the moving whale with an initial distance of 4 km achieved similar success. Each ambiguity volume encompassed the true and estimated distances of the whale in every scenario with high maximum ambiguity values. The largest distance



TABLE II. Localization results from different scenarios of a moving whale after incorporating the dilation filter to address the effects of whale movement on model-based estimates. Each simulation used  $\sigma_r = 0.0024$ .

Initial whale distance (km)	Whale depth range (km)	Whale movement relative to array	Straight scenario							Turn scenario					
			Max $V(x)$	True whale distance (km)	Distance estimate (km)	Distance bounds (km)	Depth estimate (km)	Depth bounds (km)	Max $V(x)$	Turn (deg)	True whale distance (km)	Distance estimate (km)	Distance bounds (km)	Depth estimate (km)	Depth bounds (km)
0	1.1–1.4	Toward	0.98	0.6	0	0–1.9	1.5	0–1.9	0.99	60	0.24	1.0	0–1.3	1.9	0–1.8
0	1.1–1.4	Away	0.97	0.6	0.8	0–1.9	1.3	0–1.9	0.95	60	0.24	0.8	0–1.3	1.0	0–1.8
0	1.1–1.4	Same	0.97	0	0.8	0–2.2	1.5	0–2.0	0.97	60	0	0.5	0–1.6	1.5	0–2.0
0	1.1–1.4	Opposite	0.95	0	0.5	0–1.4	0.9	0–1.5	0.95	60	0	0	0–1.3	1.0	0–1.5
4	1.1–1.5	Toward	0.99	3.4	3.5	1.6–7.3	1.4	0–2.0	0.99	60	2.3	3.0	2.0–3.8	2.0	0–2.0
4	1.1–1.5	Away	0.99	4.6	4.0	2.2–9.8	2.0	0–2.0	0.99	60	4.2	4.8	3.8–8.5	0.3	0–2.0
4	1.1–1.5	Same	0.99	4.0	5.0	2.7–12.8	1.4	0–2.0	0.99	60	4.0	5.3	3.7–8.2	2.0	0–2.0
4	1.1–1.5	Opposite	0.99	4.0	3.3	1.0–5.9	1.2	0–2.0	0.98	60	4.0	3.5	2.7–4.7	2.0	0–2.0

bounds occurred during a straight scenario for a whale moving, again, in the same direction as the array, [2.7, 12.8] km. Distance bounds were also much smaller for the turn scenarios compared to the straight scenarios with minimum distance bounds restricted to [2, 3.8] km for a diving whale moving toward the array. Depth estimates for all simulations included the true depth of the whale; however, they were deemed unreliable given the large depth bounds due to the limitations discussed previously.

### III. APPLICATION TO REAL ACOUSTIC DATA

#### A. Data description

Passive acoustic data were collected using a towed line array during a visual and acoustic line-transect cetacean survey conducted from July 6 to December 1, 2017, by the Pacific Islands Fisheries Science Center (PIFSC) and the Southwest Fisheries Science Center of the National Oceanic and Atmospheric Administration (NOAA) aboard the NOAA Ships *Oscar Elton Sette* and *Reuben Lasker* (Yano *et al.*, 2018). We tested the localization algorithm using two sperm whale encounters detected only acoustically on the towed line array, one collected on October 2 at 03:12 GMT and the second on November 21 at 02:00 GMT (Table III). The line arrays on both ships consisted of two sub-arrays (inline and end array) separated by 20 m (Fig. 1) (Rankin *et al.*, 2013). Each sub-array contained six hydrophones [HTI-96-MIN (High Tech, Long Beach, MS); 14–85 kHz  $\pm$  5 dB at  $-158$  dB re  $1 \text{ V}/\mu\text{Pa}$ ] spaced approximately 1 m apart, custom-built preamplifiers providing 37 dB (20–50 kHz  $\pm$  2 dB) of gain and a 1500 Hz high-pass filter,

and either a Keller (Newport News, VA) (PA7FLE) or Honeywell (Charlotte, NC) (PX2EN1XX200PSCHX) depth sensor placed within the first meter of each array.

Continuous acoustic data were sampled at 500 kHz for each hydrophone channel using an analog-to-digital converter (DAQ; SA Instrumentation, Ltd., Fife, UK) and PAMGuard software (version 2.00.10fa; Gillespie *et al.*, 2008) while simultaneously collecting vessel global positioning system (GPS) data. The acoustic data were monitored in real time for vocalizing cetaceans during daylight hours. Sperm whale acoustic encounters were logged by trained acousticians who identified sperm whales aurally using headphones and visually with a spectrogram by their unique high-amplitude, low-frequency broadband signals (Wahlberg, 2002; Møhl *et al.*, 2003).

#### B. Signal analysis

Recordings of the two sperm whale encounters selected from the 2017 survey were reviewed to confirm the presence of echolocation clicks and the type of click. The whale detected on October 2, 2017 (A221), produced regular clicks that are associated with foraging at depths below 200 m (Whitehead, 2003). The whale detected on November 21, 2017 (A352), emitted slow clicks indicating the presence of a male sperm whale typically located between depths of 0 and 300 m (Jaquet *et al.*, 2001; Oliveira *et al.*, 2013). The click types offered information about the behavioral state of the sperm whale and provided context for the click detection results.

TABLE III. Two sperm whale acoustic encounters localized during a cetacean abundance line-transect survey in 2017 using the model-based approach for short-aperture towed line array data. Ship location is at the time of first detection.

NOAA research vessel	Acoustic encounter ID	Click type	Ship latitude (deg)	Ship longitude (deg)	Start time GMT	Duration (min)	Number of detections
<i>Reuben Lasker</i>	A221	Regular	23.8276	-160.8906	10/18/2017 17:51	37	1082
<i>Reuben Lasker</i>	A352	Slow	23.7101	-160.4455	11/21/2017 2:00	61	167

Acoustic data were downsampled from 500 to 50 kHz prior to analysis. We implemented a simple threshold detector to prioritize speed and robustness over optimal performance in the click detection phase. For each 1-min recording, the signal was filtered with a fourth-order Butterworth bandpass filter using 2 and 15 kHz as the lower and upper cutoff frequencies to reduce noise. The envelope of the entire filtered time series was computed for each channel using a Hilbert transform. Taking the maximum envelope across all channels increased the probability of detecting the directional sperm whale clicks (Møhl *et al.*, 2003). The detector threshold was empirically determined based on the acoustic data.

We used standard cross correlation (Knapp and Carter, 1976) to measure TDOAs from the acoustic data. The TDOAs for all detections across all hydrophone pairs were estimated from cross correlation peaks. The resulting TDOA sets were noisy, but scatterplots of TDOAs over detection time clearly showed the persistent TDOA tracks corresponding to sperm whale echolocation clicks among detections of other sources. For localization, we selected the persistent TDOA tracks from the two hydrophones with the largest separation (31.1 m) that occurred along straight segments of the trackline since any TDOAs calculated during a turn would introduce more error than could be accounted for using this method. The persistent tracks were manually selected from scatterplots using a graphical data selection tool (*selectdata*; D’Errico, 2007) (Fig. 6). Selected TDOAs were smoothed and subsampled using 1-min intervals over the duration of the acoustic encounter to reduce the noise in TDOA measurements and maintain the independence between  $V_j(\mathbf{x})$ .

Ambiguity volumes were generated using a grid that varied in extent according to the geographical range of the acoustic encounter. For the foraging whale, we used the same grid resolution as in the simulation, 50 m horizontal and vertical spacing and a vertical limit of 2 km. For the slow clicking whale, we used the same horizontal and vertical spacing of 50 m but constrained the vertical limit to 0.5 km based on the available biological information. Sound

speed profiles were concatenated for the day of each encounter using the same methods as described in Sec. II. The same  $\sigma_t$  and threshold values as the simulation study were incorporated along with the dilation filter to account for potential whale movement in the localization of each real acoustic sperm encounter.

### C. Localization results

Both encounters occurred entirely along straight segments of trackline and therefore resulted in location estimates with left/right ambiguity. We continued to use 95% confidence intervals to evaluate the position bounds from the ambiguity volumes. Location estimates for the sperm whale encountered on October 18, 2017, resulted in symmetrical columnar ambiguity volumes with left/right ambiguous distance estimates of 2 [0.3, 3.8] km [ $\max V(\mathbf{x}) = 0.93$ ] and depth of 1.9 [0, 2.0] km. This example showed a noticeable offset in the trackline that likely occurred due to normal variation in set and drift of the ship [Fig. 7(a)]. This offset did not appear to significantly affect the measurements from the ambiguity volume as this type of variation is accounted for within the position bounds. Figure 7(b) also demonstrated the effects of trackline variation on the 2D bearings, where a series of disjointed bearings was produced, making it difficult to pinpoint a location and distance of the whale and likely overestimating the results. During real-time operations, the point of convergence of 2D bearing lines estimated the whale to be located at a distance of 3.1 km. While the point estimate for distance is coincidentally included within the model-based position bounds, 2D TMA does not quantify the associated uncertainty related to depth and other error sources.

The TDOAs from the slow clicks of a whale detected on November 21, 2017, produced slightly asymmetrical columnar ambiguity volumes due to a slight offset in the trackline. The ambiguity volumes also capture the effects of sound propagation to help visualize where the whale could not physically be detected within the shadow zone (Fig. 3). The left/right ambiguous distances estimated the whale to

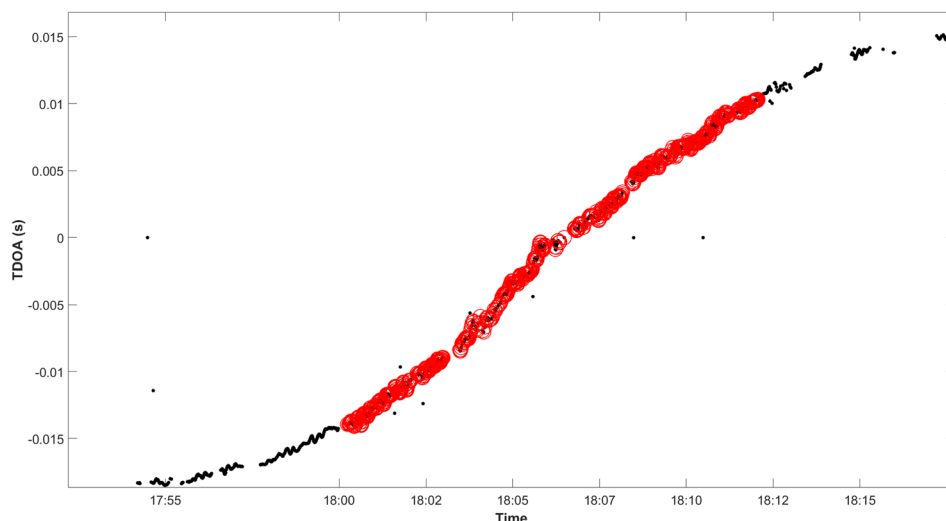


FIG. 6. (Color online) The TDOAs from click detections and noise (black dots) were manually subsetted to only include clicks within a shorter time window, around TDOA = 0 s (red circles), to improve the accuracy of the localized position estimates.

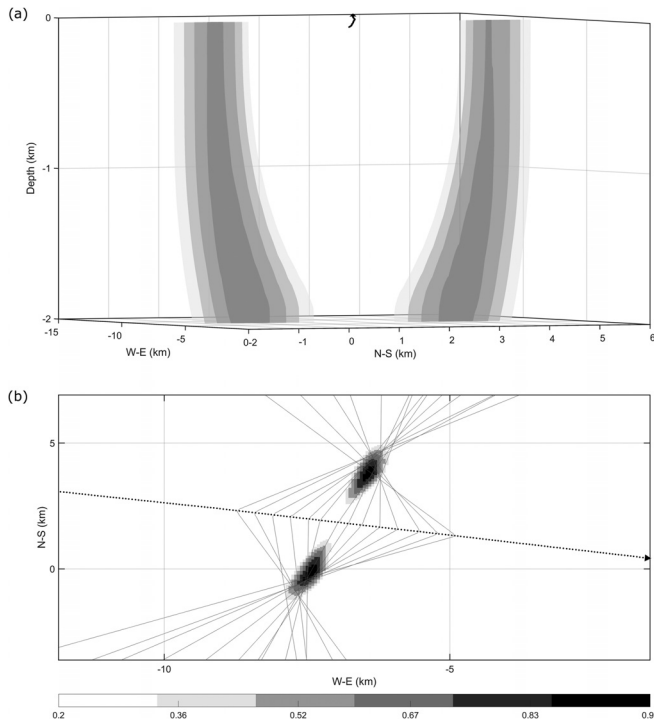


FIG. 7. A sperm whale acoustically localized on October 18, 2017, produced an ambiguity volume (a) ( $\max V(x) = 0.93$ ) estimating the whale to be 2 [0.3, 3.8] km from the trackline with left/right ambiguity at a depth of 1.9 [0, 2.0] km. The profiled ambiguity volume (b) is shown with gray lines to denote the 2D bearing lines generated using 2D TMA. The top-down view of the volume profiled over depth shows the difference between the 2D bearings and the 3D surface (b).

be 7.8 [4.1, 9.3] km off the right side and 7.0 [4.4, 9.4] km off the left side at a depth of 0.45 [0, 0.5] km [ $\max V(x) = 0.99$ ; Fig. 8]. Distance estimates measured in real-time with 2D TMA placed the whale at 7.7 km, which falls within the range of the position bounds. As in the previous example, the 2D TMA estimate does not provide error estimates.

IV. DISCUSSION

Estimating the location and distances of diving cetaceans is challenging using towed hydrophone array data due to various sources of error that introduce uncertainty and bias. We demonstrated a model-based approach for localizing deep-diving sperm whales detected using a short-aperture towed line array. The method incorporated multiple error sources to compute ambiguity volumes that represented all possible locations of the whale within a probability range based on TDOAs between the direct arrivals of echolocation clicks. The ambiguity volumes accounted for whale depth and provided position bounds to quantify the error associated with perpendicular distance and depth estimates. The framework of the model-based approach is also flexible to accommodate data collected with non-linear and large-aperture arrays that may improve position bounds.

The simulation experiments examined several parameters known to affect the localization of a diving sperm whale

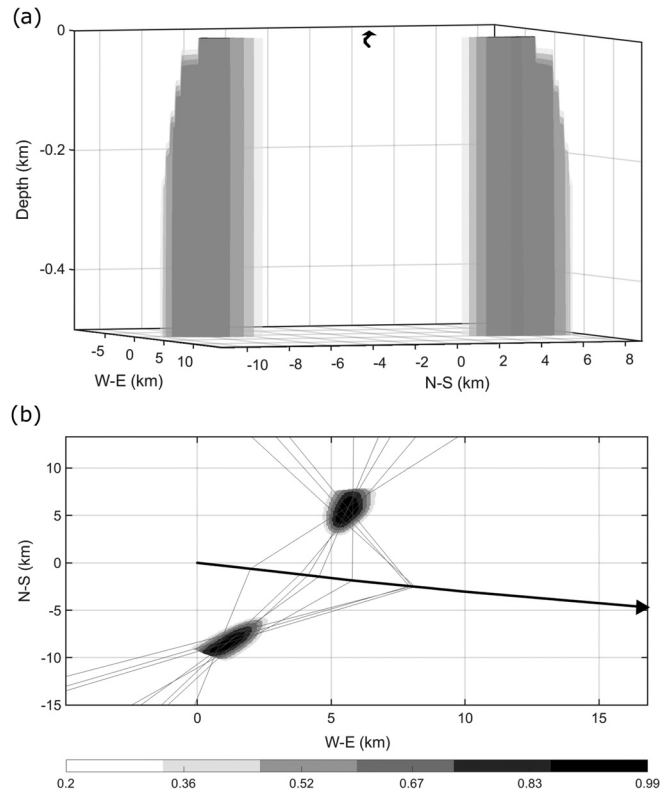


FIG. 8. Ambiguity volumes for a sperm whale detected on November 21, 2017, estimated the whale to be 7.8 km off the right side ([4.1, 9.3] km position bounds) and 7.0 km off the left side ([4.4, 9.4] km position bounds) at a depth of 0.45 km ([0, 0.5] km position bounds;  $\max V(x) = 0.99$ ). The profiled ambiguity volume (b) is shown with gray lines to denote the 2D bearing lines generated using 2D TMA. The top-down view of the volume shows the overlap between the 2D bearings and the 3D volumes (b).

and found that the ambiguity volume’s shape greatly depended on the distance, depth, ship trajectory, and movement of the whale relative to the trackline. If detected along a straight ship trajectory, a stationary whale closer to the trackline generally resulted in a U-shaped ambiguity volume [Fig. 4(1a)]. A stationary whale located farther away tended to produce two column-like volumes on either side of the trackline [Fig. 5(1a)]. Turning the ship reduced the error in the distance estimates and did not always improve the error in depth, but the model-based localization method is capable of incorporating the depth uncertainty within the position bounds of the location estimates. We now have a better understanding of the overall effects of the uncertainties on distance and depth estimates of sperm whales detected on short-aperture towed line arrays, which may be useful for future surveys.

Our model-based localization method provides more informed distance estimates for deep-diving sperm whales compared to estimates from conventional 2D TMA methods. The semi-automated process we developed for calculating the ambiguity volumes contributes a generalized method for incorporating errors and objectively localizing whales in three dimensions for towed array systems. The real acoustic encounter of the closer whale (Fig. 7) highlighted the differences between subjectively choosing locations based on

disjointed 2D bearings and automatically estimating them from the ambiguity volume. The 2D bearings are more likely to overestimate the distance of closer whales compared to whales located farther away (Fig. 8), but in both instances, the estimates from 2D TMA do not account for uncertainties when localizing whales at depth. The distance estimates [at max  $V(x)$ ] may be utilized to compute a detection function for abundance estimation, but additional theoretical development is necessary to estimate an error model for incorporating the distance bounds.

A major limitation to reducing the depth bounds in the current simulated and real acoustic data sets is the lack of surface reflections, which is attributed to the shallow array depth, small hydrophone spacing, linear configuration of hydrophones, and long-duration echolocation clicks. However, the model-based framework can be generalized to incorporate surface reflections when available from other deep-diving species. For example, the surface reflections from beaked whale species may be used to compute ambiguity volumes to achieve more precise distance and depth bounds (Zimmer *et al.*, 2008; DeAngelis *et al.*, 2017). The surface reflections would be treated as arriving on a “virtual” hydrophone positioned at an elevation above the ocean surface equivalent to the array depth, which would result in an additional hydrophone pair. Ambiguity volumes computed from surface-reflected clicks could be combined with ambiguity volumes from direct-arrival clicks via multiplication [Eq. (1)]. The model-based approach would also be useful for localizing beaked whales in the absence of surface-reflected clicks since they are typically detected at depths  $>1$  km within close range relative to the array ( $\sim 2$  km; Barlow *et al.*, 2013).

The resolution and extent of the spatial grid used to generate the ambiguity volumes can also affect the localization results and may depend on the study area. The spatial resolution of the grid will affect the precision of the estimates and should be selected based on the specific needs of the application. Finer resolutions will provide more precise position bounds for estimates than coarser resolutions but are more computationally intensive. We chose a spatial grid with a horizontal and vertical spacing of 50 m because position bounds for distance estimates were smaller than coarser grid resolutions and similar to finer grid resolutions at a lower computational cost. The extent of the grid assumes that it is physically impossible for the animals to be located beyond a certain range. For deep-diving cetaceans, the extent of the  $z$  dimension is an important consideration. In this application, we selected a vertical extent of 2 km based on available dive tag data for sperm whales. Several factors should be considered when selecting the extent of the spatial grid (e.g., the detection range, the environment, animal behavior) to ensure estimates are relevant to the species and study area.

Sound propagation effects are an important consideration in any localization method as they will affect the range at which sound can be detected depending on the depth of the hydrophones (Chapman, 2004; Tiemann *et al.*, 2004; Thode, 2005; Zimmer, 2013; von Benda-Beckmann *et al.*,

2018). For instance, the shadow zone is the region where sound rays are refracted and fail to propagate in a direct path to the receiver. Its extent depends on the oceanographic conditions of the study area and limits the detection range of a sound source. For example, in Hawaiian waters, it is unlikely that whales vocalizing at depths less than 0.4 km will be detected on a near-surface line array beyond approximately 9 km distance (Fig. 3). The effects of sound propagation are noticeable in the slow clicking whale example (Fig. 8), where the edges of the ambiguity volume are tapered according to the edge of the shadow zone. We now have a better understanding of the influence of sound propagation effects on the localization of sperm whales and other deep-diving cetaceans in Hawaiian waters. The model-based localization approach can incorporate sound speed profiles for any study area to account for the effects of sound propagation when localizing towed array data.

Moving whale simulations resulted in larger position bounds from the dilated ambiguity volumes, which we found to be appropriate when the assumptions of a stationary source are violated. One advantage of the model-based approach includes the ability to incorporate and quantify the increase in uncertainty due to animal movement. The horizontal and vertical speeds used to parameterize the dilation filter conservatively represented all possible movement of a diving whale. The four directions of travel at a constant swim speed also depicted more dramatic examples of whale movement, which can be more static or variable depending on the whale’s behavioral state (Whitehead, 2003). Nonetheless, despite the extreme simulated movement patterns, the true locations of the whales were successfully estimated within the more conservative position bounds.

The simulation experiments and real-data examples only included localization results for individual whales. In tropical and subtropical oceans, sperm whales frequently congregate in social groups with multiple animals diving asynchronously to forage (Whitehead, 1996). The model-based localization approach is capable of iteratively localizing multiple animals within a group provided that TDOA tracks can be separated, but the overall distance estimate for the group may depend on the group’s geographical spread. When visual observers estimate distances to large groups of dolphins spread over hundreds of meters, the distances to the centers of the groups are utilized in distance sampling methods. A similar approach could be applied in the case of localizing multiple deep-diving whales. Further simulation experiments are needed to test this theory and include appropriate parameters and errors to fully evaluate the capabilities of the model-based approach in this context.

The use of short-aperture towed line arrays to acoustically localize sperm whales and other deep-diving species is ubiquitous, but most studies rely on 2D TMA to calculate point estimates for distance without considering the depth of the animals or the various sources of uncertainty (Leaper *et al.*, 1992; Gillespie and Leaper, 1997; Barlow and Taylor, 2005; Lewis *et al.*, 2007; Yack *et al.*, 2013; Yack *et al.*, 2016; Wild *et al.*, 2017; Fleming *et al.*, 2018; Yano *et al.*, 2018). One benefit of

2D TMA is its ability to track and localize vocalizing cetaceans in real time during line-transect surveys (Rankin *et al.*, 2008). It is possible to integrate the model-based approach presented here into real-time applications for more precise tracking and localization of deep-diving species with position bounds. The computational burden [ $\sim 3\text{--}10$  min per  $V(\mathbf{x})$  in our implementation] may be acceptable for some applications and could be reduced with increased computational power and more optimized code. A benefit of the method presented here is that it can be generalized for any towed hydrophone configuration, and the semi-automated workflow requires minimal user-input to reduce subjectivity and improve the reproducibility of localization results. As abundance estimation techniques continue to evolve for PAM data, these qualities will be essential for generating the distance data required for acoustic abundance estimation of deep-diving cetaceans from line-transect survey data. Understanding the effects of the uncertainties on localization results also helps identify data limitations to guide future PAM system design and data collection methods. Overall, the model-based localization approach provides a simple mathematical framework for incorporating the uncertainties inherent in towed hydrophone array data for more robust localization of deep-diving cetaceans.

#### ACKNOWLEDGMENTS

The acoustic data examples included in this analysis were collected aboard the R/V *Reuben Lasker* thanks to the hard work and dedication of the scientists and crew. We would like to extend special thanks to Jennifer L. K. McCollough, Shannon Coates, Anne Simonis, and Jessica Crance for facilitating the acoustic data collection. The survey was funded by PIFSC, NOAA Fisheries Office of Protected Resources, NOAA Fisheries Office of Science and Technology, Chief of Naval Operation Environmental Readiness Division and Pacific Fleet, and Bureau of Ocean Energy Management. Acoustic data analysis was funded by PIFSC and the National Science Foundation Graduate Research Fellowships Program. We thank Pina Gruden and Fábio Casagrande Hirono for their thoughtful comments on an earlier version of the manuscript. We also thank the three anonymous reviewers for their very helpful suggestions that helped improve and clarify our manuscript.

Aoki, K., Amano, M., Sugiyama, N., Muramoto, H., Suzuki, M., Yoshioka, M., Mori, K., Tokuda, D., and Miyazaki, N. (2007). "Measurement of swimming speed in sperm whales," in *Proceedings of the International Symposium on Underwater Technology, UT 2007—International Workshop on Scientific Use of Submarine Cables and Related Technologies 2007*, April 17–20, Tokyo, Japan, pp. 467–471.

Barlow, J., and Taylor, B. L. (2005). "Estimates of sperm whale abundance in the northeastern temperate Pacific from a combined acoustic and visual survey," *Mar. Mamm. Sci.* **21**(3), 429–445.

Barlow, J., Tyack, P. L., Johnson, M. P., Baird, R. W., Schorr, G. S., Andrews, R. D., and Aguilar de Soto, N. (2013). "Trackline and point detection probabilities for acoustic surveys of Cuvier's and Blainville's beaked whales," *J. Acoust. Soc. Am.* **134**(3), 2486–2496.

Baumann-Pickering, S., McDonald, M. A., Simonis, A. E., Berga, A. S., Merckens, K. P. B., Oleson, E. M., Roch, M. A., Wiggins, S. M., Rankin, S., Yack, T. M., and Hildebrand, J. A. (2013). "Species-specific beaked whale echolocation signals," *J. Acoust. Soc. Am.* **134**(3), 2293–2301.

Bittle, M., and Duncan, A. (2013). "A review of current marine mammal detection and classification algorithms for use in automated passive acoustic monitoring," in *Proceedings of the Annual Conference of the Australian Acoustical Society 2013, Acoustics 2013: Science, Technology and Amenity*, November 17–20, Victor Harbor, Australia.

Bossart, G. D. (2011). "Marine mammals as sentinel species for oceans and human health," *Vet. Pathol.* **48**(3), 676–690.

Boyer, T. P., Antonov, J. I., Baranova, O. K., Coleman, C., Garcia, H. E., Grodsky, A., Johnson, D. R., Locarnini, R. A., Mishonov, A. V., O'Brien, T. D., Paver, C. R., Reagan, J. R., Seidov, D., Smolyar, I. V., and Zweng, M. M. (2013). *World Ocean Database 2013: NOAA Atlas NESDIS 72*, edited by S. Levitus and A. Mishonov (National Oceanographic Data Center, Silver Spring, MD).

Buckland, S. T., Anderson, D. R., Burnham, K. P., Laake, J. L., Borchers, D. L., and Thomas, L. (2001). *Introduction to Distance Sampling Estimating Abundance of Biological Populations* (Oxford University, New York).

Carlén, I., Thomas, L., Carlström, J., Amundin, M., Teilmann, J., Tregenza, N., Tougaard, J., Koblit, J. C., Sveegaard, S., Wennerberg, D., Loisa, O., Dähne, M., Brundiers, K., Kosecka, M., Kyhn, L. A., Ljungqvist, C. T., Pawliczka, I., Koza, R., Arciszewski, B., Galatius, A., Jabbusch, M., Laaksonlaita, J., Niemi, J., Lyytinen, S., Gallus, A., Benke, H., Blankett, P., Skóra, K. E., and Acevedo-Gutiérrez, A. (2018). "Basin-scale distribution of harbour porpoises in the Baltic Sea provides basis for effective conservation actions," *Biol. Conserv.* **226**, 42–53.

Chapman, D. M. F. (2004). "You can't get there from here: Shallow water sound propagation and whale localization," *Can. Acoust.* **32**(2), 167–171.

Davis, G. E., Baumgartner, M. F., Bonnell, J. M., Bell, J., Berchok, C., Bort Thornton, J., Brault, S., Buchanan, G., Charif, R. A., Cholewiak, D., Clark, C. W., Corkeron, P., Delarue, J., Dudzinski, K., Hatch, L., Hildebrand, J., Hodge, L., Klinck, H., Kraus, S., Martin, B., Mellinger, D. K., Moors-Murphy, H., Nieuwkerk, S., Nowacek, D. P., Parks, S., Read, A. J., Rice, A. N., Risch, D., Širović, A., Soldevilla, M., Stafford, K., Stanistreet, J. E., Summers, E., Todd, S., Warde, A., and Van Parijs, S. M. (2017). "Long-term passive acoustic recordings track the changing distribution of North Atlantic right whales (*Eubalaena glacialis*) from 2004 to 2014," *Sci. Rep.* **7**(1), 13460.

DeAngelis, A. I., Valtierra, R., Van Parijs, S. M., and Cholewiak, D. (2017). "Using multipath reflections to obtain dive depths of beaked whales from a towed hydrophone array," *J. Acoust. Soc. Am.* **142**(2), 1078–1087.

D'Errico, J. (2007). Graphical data selection tool (Version 1.0.0.0) MATLAB Central (<https://www.mathworks.com/matlabcentral/fileexchange/13857-graphical-data-selection-tool>).

Fleming, A. H., Yack, T., Redfern, J. V., Becker, E. A., Moore, T. J., and Barlow, J. (2018). "Combining acoustic and visual detections in habitat models of Dall's porpoise," *Ecol. Modell.* **384**, 198–208.

Gebbie, J., Siderius, M., and Allen, J. S. (2015). "A two-hydrophone range and bearing localization algorithm with performance analysis," *J. Acoust. Soc. Am.* **137**(3), 1586–1597.

Gero, S., Whitehead, H., and Rendell, L. (2016). "Individual, unit and vocal clan level identity cues in sperm whale codas," *R. Soc. Open Sci.* **3**(1), 150372.

Gibb, R., Browning, E., Glover-Kapfer, P., and Jones, K. E. (2019). "Emerging opportunities and challenges for passive acoustics in ecological assessment and monitoring," *Methods Ecol. Evol.* **10**(2), 169–185.

Gillespie, D., and Leaper, R. (1997). "An acoustic survey for sperm whales in the Southern Ocean Sanctuary conducted from the RSV Aurora Australis," Report No. 47 (International Whaling Commission, Cambridge, UK), pp. 897–907.

Gillespie, D., Mellinger, D. K., Gordon, J., McLaren, D., Redmond, P., McHugh, R., Trinder, P. W., Deng, X. Y., and Thode, A. (2008). "PAMGUARD: Semiautomated, open source software for real-time acoustic detection and localisation of cetaceans," *J. Acoust. Soc. Am.* **30**(5), 54–62.

Gonzalez, R. C., Woods, R. E., and Eddins, S. L. (2009). *Digital Image Processing Using MATLAB* (Gatesmark Publishing, Knoxville, TN).

Harris, D. V., Miksis-Olds, J. L., Vernon, J. A., and Thomas, L. (2018). "Fin whale density and distribution estimation using acoustic bearings derived from sparse arrays," *J. Acoust. Soc. Am.* **143**(5), 2980–2993.

Hazen, E. L., Abrahms, B., Brodie, S., Carroll, G., Jacox, M. G., Savoca, M. S., Scales, K. L., Sydeman, W. J., and Bograd, S. J. (2019). "Marine top predators as climate and ecosystem sentinels," *Front. Ecol. Environ.* **17**, 565–574.

- Hildebrand, J. A. (2005). "Impacts of anthropogenic sound," in *Marine Mammal Research: Conservation beyond Crisis*, edited by J. E. Reynolds III, W. F. Perrin, R. R. Reeves, S. Montgomery, and T. J. Ragen (Johns Hopkins University, Baltimore, MD), pp. 101–124.
- Hildebrand, J. A., Frasier, K. E., Baumann-Pickering, S., Wiggins, S. M., Merckens, K. P., Garrison, L. P., Soldevilla, M. S., and McDonald, M. A. (2019). "Assessing seasonality and density from passive acoustic monitoring of signals presumed to be from pygmy and dwarf sperm whales in the Gulf of Mexico," *Front. Mar. Sci.* **6**, 1–17.
- Hodge, L. E. W., Baumann-Pickering, S., Hildebrand, J. A., Bell, J. T., Cummings, E. W., Foley, H. J., McAlarney, R. J., McLellan, W. A., Pabst, D. A., Swaim, Z. T., Waples, D. M., and Read, A. J. (2018). "Heard but not seen: Occurrence of *Kogia* spp. along the western North Atlantic shelf break," *Mar. Mamm. Sci.* **34**(4), 1141–1153.
- Irvine, L., Palacios, D. M., Urbán, J., and Mate, B. (2017). "Sperm whale dive behavior characteristics derived from intermediate-duration archival tag data," *Ecol. Evol.* **7**(19), 7822–7837.
- Jaquet, N., Dawson, S., and Douglas, L. (2001). "Vocal behavior of male sperm whales: Why do they click?," *J. Acoust. Soc. Am.* **109**(5 Pt. 1), 2254–2259.
- Knapp, C., and Carter, G. (1976). "The generalized correlation method for estimation of time delay," *IEEE Trans. Acoust. Speech Signal Proc.* **24**(4), 320–327.
- Leeper, R., Chappell, J., and Gordon, J. (1992). *The Development of Practical Techniques for Surveying Sperm Whale Populations Acoustically* (University of Oxford, Oxford, UK).
- Lewis, T., Gillespie, D., Lacey, C., Matthews, J., Danbolt, M., Leaper, R., McLanaghan, R., and Moscrop, A. (2007). "Sperm whale abundance estimates from acoustic surveys of the Ionian Sea and Straits of Sicily in 2003," *J. Mar. Biol. Assoc. UK* **87**(1), 353–357.
- Madsen, P. T., Wahlberg, M., and Møhl, B. (2002). "Male sperm whale (*Physeter macrocephalus*) acoustics in a high-latitude habitat: Implications for echolocation and communication," *Behav. Ecol. Sociobiol.* **53**(1), 31–41.
- Marcoux, M., Whitehead, H., and Rendell, L. (2006). "Coda vocalizations recorded in breeding areas are almost entirely produced by mature female sperm whales (*Physeter macrocephalus*)," *Can. J. Zool.* **84**, 609–614.
- Marques, T. A., Thomas, L., Martin, S. W., Mellinger, D. K., Ward, J. A., Moretti, D. J., Harris, D., and Tyack, P. L. (2013). "Estimating animal population density using passive acoustics," *Biol. Rev.* **88**(2), 287–309.
- Marques, T. A., Thomas, L., Ward, J., DiMarzio, N., and Tyack, P. L. (2009). "Estimating cetacean population density using fixed passive acoustic sensors: An example with Blainville's beaked whales," *J. Acoust. Soc. Am.* **125**(4), 1982–1994.
- MATLAB (2018). Version 9.5.0 (R2019b) (MathWorks Inc., Natick, MA).
- Miller, P. J. O., Johnson, M. P., and Tyack, P. L. (2004). "Sperm whale behaviour indicates the use of echolocation click buzzes 'creaks' in prey capture," *Proc. Biol. Sci.* **271**(1554), 2239–2247.
- Møhl, B., Wahlberg, M., Madsen, P. T., Heerfordt, A., and Lund, A. (2003). "The monopolised nature of sperm whale clicks," *J. Acoust. Soc. Am.* **114**(2), 1143–1154.
- Moore, S. E. (2008). "Marine mammals as ecosystem sentinels," *J. Mammal.* **89**(3), 534–540.
- Nosal, E.-M. (2013). "Model-based marine mammal localization methods," in *Detection Classification Localization of Marine Mammals Using Passive Acoustics: 2003–2013, 10 Years of International Research* (Dirac NGO, Paris), pp. 173–183.
- Nosal, E.-M., and Frazer, L. N. (2006). "Track of a sperm whale from delays between direct and surface-reflected clicks," *Appl. Acoust.* **67**(11), 1187–1201.
- Nosal, E.-M., and Frazer, L. N. (2007). "Sperm whale three-dimensional track, swim orientation, beam pattern, and click levels observed on bottom-mounted hydrophones," *J. Acoust. Soc. Am.* **122**(4), 1969–1978.
- Oliveira, C., Wahlberg, M., Johnson, M., Miller, P. J., and Madsen, P. T. (2013). "The function of male sperm whale slow clicks in a high latitude habitat: Communication, echolocation, or prey debilitation?," *J. Acoust. Soc. Am.* **133**(5), 3135–3144.
- Oliveira, C., Wahlberg, M., Silva, M. A., Johnson, M., Antunes, R., Wisniewska, D. M., Fais, A., Gonçalves, J., and Madsen, P. T. (2016). "Sperm whale codas may encode individuality as well as clan identity," *J. Acoust. Soc. Am.* **139**(5), 2860–2869.
- Porter, M. B. (2011). *The BELLHOP Manual and User's Guide: Preliminary Draft* (Heat, Light, and Sound Research, La Jolla, CA).
- Porter, M. B., and Liu, Y.-C. (1994). "Finite-element ray tracing," *Theor. Comput. Acoust.* **2**, 947–956.
- Rankin, S., Barlow, J., Barkley, Y., and Valtierra, R. (2013). "A guide to constructing hydrophone arrays for passive acoustic data collection during NMFS shipboard cetacean surveys," NOAA Technical Memorandum NMFS-SWFSC-511 (U.S. Department of Commerce, Washington, DC).
- Rankin, S., Barlow, J., and Oswald, J. N. (2008). "An assessment of the accuracy and precision of localization of a stationary sound source using a two-element towed hydrophone array," NOAA Technical Memorandum NMFS-SWFSC-416 (U.S. Department of Commerce, Washington, DC).
- Rendell, L., and Whitehead, H. (2004). "Do sperm whales share coda vocalizations? Insights into coda usage from acoustic size measurement," *Anim. Behav.* **67**(5), 865–874.
- Schorr, G. S., Falcone, E. A., Moretti, D. J., and Andrews, R. D. (2014). "First long-term behavioral records from Cuvier's beaked whales (*Ziphius cavirostris*) reveal record-breaking dives," *PLoS One* **9**, e92633.
- Teloni, V., Johnson, M. P., Miller, P. J. O., and Madsen, P. T. (2008). "Shallow food for deep divers: Dynamic foraging behavior of male sperm whales in a high latitude habitat," *J. Exp. Mar. Biol. Ecol.* **354**(1), 119–131.
- Thode, A. (2004). "Tracking sperm whale (*Physeter macrocephalus*) dive profiles using a towed passive acoustic array," *J. Acoust. Soc. Am.* **116**(1), 245–253.
- Thode, A. (2005). "Three-dimensional passive acoustic tracking of sperm whales (*Physeter macrocephalus*) in ray-refracting environments," *J. Acoust. Soc. Am.* **118**(6), 3575–3584.
- Tiemann, C. O., Porter, M. B., and Frazer, L. N. (2004). "Localization of marine mammals near Hawaii using an acoustic propagation model," *J. Acoust. Soc. Am.* **115**(6), 2834–2843.
- Van Parijs, S. M., Clark, C. W., Sousa-Lima, R. S., Parks, S. E., Rankin, S., Risch, D., and Van Opzeeland, I. C. (2009). "Management and research applications of real-time and archival passive acoustic sensors over varying temporal and spatial scales," *Mar. Ecol. Prog. Ser.* **395**, 21–36.
- von Benda-Beckmann, A. M., Thomas, L., Tyack, P. L., and Ainslie, M. A. (2018). "Modelling the broadband propagation of marine mammal echolocation clicks for click-based population density estimates," *J. Acoust. Soc. Am.* **143**(2), 954–967.
- Wahlberg, M. (2002). "The acoustic behaviour of diving sperm whales observed with a hydrophone array," *J. Exp. Mar. Biol. Ecol.* **281**(1), 53–62.
- Warner, G. A., Dosso, S. E., and Hannay, D. E. (2017). "Bowhead whale localization using time-difference-of-arrival data from asynchronous recorders," *J. Acoust. Soc. Am.* **141**(3), 1921–1935.
- Watwood, S. L., Miller, P. J. O., Johnson, M., Madsen, P. T., and Tyack, P. L. (2006). "Deep-diving foraging behaviour of sperm whales (*Physeter macrocephalus*)," *J. Anim. Ecol.* **75**(3), 814–825.
- Whitehead, H. (1996). "Babysitting, dive synchrony, and indications of alloparental care in sperm whales," *Behav. Ecol. Sociobiol.* **38**(4), 237–244.
- Whitehead, H. (2003). *Sperm Whales: Social Evolution in the Ocean* (University of Chicago, Chicago).
- Whitehead, H., and Weilgart, L. (1990). "Click rates from sperm whales," *J. Acoust. Soc. Am.* **87**(4), 1798–1806.
- Wild, L., Straley, J., and Gordon, J. (2017). *Real Time Localization of Sperm Whales Using a Towed Array Hydrophone* (Alaska Longline Fishermen's Association, Sitka, AK).
- Yack, T. M., Barlow, J., Calambokidis, J., Avenue, W., and Coates, S. (2013). "Passive acoustic monitoring using a towed hydrophone array results in identification of a previously unknown beaked whale habitat," *J. Acoust. Soc. Am.* **134**(3), 2589–2595.
- Yack, T. M., Norris, T. N., and Novak, N. (2016). *Acoustic Based Habitat Models for Sperm Whales in the Mariana Islands Region* (Bio-Waves, Arlington, VA).
- Yano, K. M., Oleson, E. M., Keating, J. L., Ballance, L. T., Hill, M. C., Bradford, A. L., Allen, A. N., Joyce, T. W., Moore, E., and Henry, A. (2018). "Cetacean and seabird data collected during the Hawaiian Islands Cetacean and Ecosystem Assessment Survey (HICEAS), July–December 2017," NOAA Technical Memorandum NMFS-PIFSC-72 (U.S. Department of Commerce, Washington, DC).
- Zimmer, W. M. X. (2013). "Range estimation of cetaceans with compact volumetric arrays," *J. Acoust. Soc. Am.* **134**(3), 2610–2618.
- Zimmer, W. M. X., Harwood, J., Tyack, P. L., Johnson, M. P., and Madsen, P. T. (2008). "Passive acoustic detection of deep-diving beaked whales," *J. Acoust. Soc. Am.* **124**(5), 2823–2832.